Hybrid, multiresolution wires with massless frictional contacts

Martin Servin, Claude Lacoursière, Fredrik Nordfelth and Kenneth Bodin

***Abstract*—We describe a method for the visual interactive simulation of wires contacting with rigid multibodies. The physical model used is a hybrid combining lumped elements and massless quasistatic representations. The latter is based on a kinematic constraint preserving the total length of the wire along a segmented path which can involve multiple bodies simultaneously and dry frictional contact nodes used for roping, lassoing and fastening. These nodes provide stick and slide friction along edges of the contacting geometries. The lumped element resolution is adapted dynamically based on local stability criteria, becoming coarser as the tension increases, and up to the purely kinematic representation. Kinematic segments and contact nodes are added and deleted and propagated based on contact geometries and dry friction configurations. The method gives dramatic increase on both performance and robustness because it quickly decimates superfluous nodes without loosing stability, yet adapts to complex configurations with many contacts and high curvature, keeping a fixed, large integration time step. Numerical results demonstrating the performance and stability of the adaptive multiresolution scheme are presented along with an array of representative simulation examples illustrating the versatility of the frictional contact model.**

I. Introduction

Computer graphics animations based on physics simulation have proved useful in a variety of applications including interactive training simulators, computer games, and visual effects used in motion pictures. The need for both realism and artistic license has lead to an increasing repertoire of physics models from the classic point particles and rigid bodies to continuous solids, membranes and cables, the subject of the present article. There is a demand both for simultaneous simulations and coupling of all existing models and techniques, and for increased spatial resolution. More detailed and sophisticated geometries are used to improve visual quality but also produce more complex contact configurations. This puts constant pressure to reduce the computational costs which could explode polynomially without novel numerical methods. If there is no compromise on the spatial resolution, the most obvious economy is the increase in the integration time step. But higher spatial resolution means many more, smaller and lighter elements. This brings high frequency oscillation modes causing instabilities in numerical time integrators. At finite energy, high frequency oscillations have low spatial amplitude which are practically invisible to the naked eye. Adaptive resolution is a way to filter out these to save computational time and maintain stability. This is the approach chosen here for the specific example of wires and provided with a consistent method for handling dynamical and frictional contacts.

M. Servin, K. Bodin and C. Lacoursière are with Umeå University.
E-mail: martin.servin@physics.umu.se
F. Nordfelth is with Algoryx Simulation.

What we call a wire is a long thin and flexible object. This includes cables, strings, chains, ropes, etc., all of which have their own special properties but share important features. Each of these corresponds to interesting numerical problems with regards to efficiency, stability and accuracy. The first issue is the spatial discretization. It is necessary to produce smooth curves with radius of curvature potentially as small as the cross section to produce the most visually compelling results. But since this is negligible with respect to the length of the wire, a uniform discretization is impractical for anything but short strands, something already mentioned in previous work[1]. Second, there is dynamics on several time scales, typically orders in magnitude apart, that must be either resolved by the time integrator or filtered out not to cause numerical instabilities. These time scales include fast sound propagation in dense material, i.e., compressional waves propagating along the wire faster than $1000\ m/s^2$, moderate transversal vibrations that typically range between 0.1–1000 Hz, slow mode oscillations caused by a heavy load that makes the wire uniformly elongate or swing from side to side with the load, typically 0.001–1 Hz. In the visual context, the sound propagation can be assumed instantaneous and need not be resolved. The transversal vibration modes are interesting when they have high amplitude and low frequency, e.g., slow vibrations, slacking or whipping motion, whereas the high-frequency part is not important to resolve in visual applications. A further complication is that these time scales depend on mass, length, spatial resolution and elasticity, but also on initial conditions and user interaction. Thirdly, wires are used to tie and lasso things which requires dry frictional contact forces. Fourth, several aspects of their dynamics involve large mass ratios. In most situations, the load on a wire is much heavier than the wire itself, let alone the lumped masses used in the discretization. High mass ratios are directly responsible for characteristic wire dynamics such as whipping, buckling, and fast loading effects. Fast loading can be seen in water skiing, both when the wire tenses during the lift phase, or when turning, or even in hair in response to a vigorous head shake. Finally, wires are versatile. They are alternately spooled, bunched, put under tension, wrapped around things, etc. A good wire model is not really useful if it cannot cover several of these very different regimes.

The context of realtime imposes a few additional stringent conditions. The first is speed, of course, since there is a hard limit on the computational budget. This implies fixed time step integration. In turn, this requires strong stability and robustness. The speed requirement also requires using as few elements as possible, i.e., only when and where the discretiza-

tion must be very fine. Many computer graphics applications also have requirements on using physical models that may be validated, parametrized with real world data and produce faithful dynamics. Examples include training simulators for vehicle operators or surgeons, virtual prototyping, and research tools used in behavioral science and medecine.

The strategy described below rests on a dynamic non-uniform spatial discretization based on local stability criteria for free segments, a quasistatic frictional contact model for roping, and lumped mass model for resolved mass distribution to enable slacking and low-frequency vibrations. Non-uniform discretization and the quasistatic contact model allow for adding many nodes where there is high curvature as well as when a wire goes over a complex geometry in which case contacts are needed at each edge to provide realism and good grip without sacrificing the computational performance or stability. In other regions and situations the resolution may be reduced to a minimum to save computational time.

The approach of combining quasistatic frictional contacts with adaptive resolution should apply also to other flexible objects common in computer graphics, e.g., cloth and volumetric deformable models, to improve the robustness and computational performance. The model can also be combined with other numerical simulation methods that are common in computer graphics than the particular one employed here. Because the method generally saves time and automatically provides high resolution where it is needed, it is expected to be useful in a broad range of graphics applications, whether they are real-time or not.

A. Related work

In computer graphics, several approaches have been presented for simulating wires. Wires can be considered as a non-linear elastic deformable object [2]. An overview of physics based deformable models in computer graphics is found in [3]. Continuum models for wires, e.g., Cosserat theory or Kirchhoff theory, introduced to computer graphics by D. K. Pai [1], have the form of partial differential equations which may be discretized, e.g., employing finite differences or finite elements. Two extensions of the Cosserat approach are particularly interesting in relation to the present paper. Bergou *et al.* [4] presented an approach where the twist deformation is treated quasistatically for increased computational efficiency and numerical robustness. Another extension by Spillmann and Teschner [5] includes a method to adaptively introduce control points when high curvature is needed, when complex contact sets are considered for instanced. The new nodes are positioned to minimize the bending energy induced by the refinement. Nodes are also deleted when high curvature is no longer needed according to user defined criteria, independent of energy or stability considerations. Alternative to continuum models is to model the wire as a chain of particles or rigid bodies connected by constraints, stiff springs or deformation potentials. Rigid body-based simulation of chain systems has been developed with techniques for adaptive contact computations [6] and simplification by joint rigidfication [7]. A spring model including resistance to both bending and twisting was presented in [8]. Modeling of elastic wires by splines subject to minimization of some assigned deformation energy shares many similarities with both the continuum based models and spring-based wires. This approach was first introduced to computer graphics in [9]. Approaches to simulate wires using reduced coordinates are computationally fast when the system has linear or tree topology and contacts are soft. This has been applied for character animation [10] and visualization of hair strands [11], where also new dynamic models for Cosserat rods were introduced.

Fast and robust methods for frictional contacts were introduced to computer graphics through the work by Baraff, e.g., [12] and [13], based on constraints and complementarity conditions for non penetration and dry friction. This approach has been both refined, e.g., by Anitescu and Potra [14], and complemented by many others, including iterative impulse based methods and projection techniques, e.g., [15] and [16].

The requirements on visual realism, computational speed, numerical robustness and faithful dynamics are difficult to meet all at once and no method has been presented that meet them all. If the real-time requirement is dropped, most methods have the potential of meeting the requirements at fine enough discretization of time and space, provided the use of a proper physical model. The cost for this is long computational time. If faithful dynamics and use of real-world parameters is dropped as a requirement there are computationally efficient and numerically robust methods for damping and projecting the positions and velocities that violate any constraints or stiff potentials. These approaches allow for large complex systems at real-time, see, e.g., [17] for an application to real-time cloth. But artificial damping and projections of large constraint violations comes with the cost of dynamics that is inconsistent with Newtonian physics and introduction of parameters with unclear relation to real-world properties. This is not necessarily a severe problem and there is sometimes artistic freedom in deviating from the laws of physics. But from a design and modeling perspective it is beneficial to use models and parameters than can be validated, found in tables of material properties or at least have very clear physical meaning. In the case of visual interactive simulations for professional training, virtual prototyping and engineering it is even crucial.

Particularly difficult features to handle are high tension events and contacts, e.g., to have a light wire supporting a load 100 times heavier than the wire and with dynamical contacts with other geometries. Simulation of such “high mass ratio” system with time step $h \sim 1/60\ s$ fails because numerical instabilities develop from high-frequency oscillations and cause jittering and undesired elongation of the wire. As the mass ratio increase the time step required for stable simulation decreases. Complex configurations and contacts with detailed geometries require high resolution which means high mass ratio. The limit of high resolution is thus associated both with increased computational complexity and requires smaller time steps. In the exploration of rigid multibody chain it was discovered that stability at indefinitely large mass ratios between load and wire can be realized by increasing the bend and twist elasticity of the wire to suppress the high frequency transversal oscillations [18]. The drawback of that approach is

the lack of a stable and fast contact method to combine it with. Another attempt to remedy the high mass ratio instability is the quasistatic *massless cable* model presented in [19] which is a many-body constraint—carrying no mass elements at all—that constrains the motion of the rigid bodies in the system to preserve the total length between the wire endpoints and via an arbitrary number of intermediate eye nodes that, in effect, allow the bodies to slide along the wire. This approach was extended in [20] to include wire oscillations superimposed on the quasistatic wire and contacts modeled as pulleys with fixed positions. The drawback of the massless cable approach is that the wire cannot slack and contacts cannot slide along the colliding geometry nor affect the body by frictional contact forces or exhibit stick-slip transition. A first extension to include mass elements with adaptive resolution was made in [21]. That approach is based on a simple *uniform* resolution algorithm, with stability condition and coarsening and refinement transition rules valid only for uniform resolution. This is a severe restriction that prohibits any practical use beyond just having a wire supporting a heavy load. None of the methods discussed above include dynamic contact nodes, and neither is there any comparative study between them. This paper also have the idea of applying adaptive resolution for optimal trade-off between robustness and computational performance, but with a much more suitable approach and takes the analysis further. In particular, non-uniform adaptive resolution and dynamical and frictional contacts, contributing to additional complementarity conditions, are new results as is the corresponding analysis of these methods.

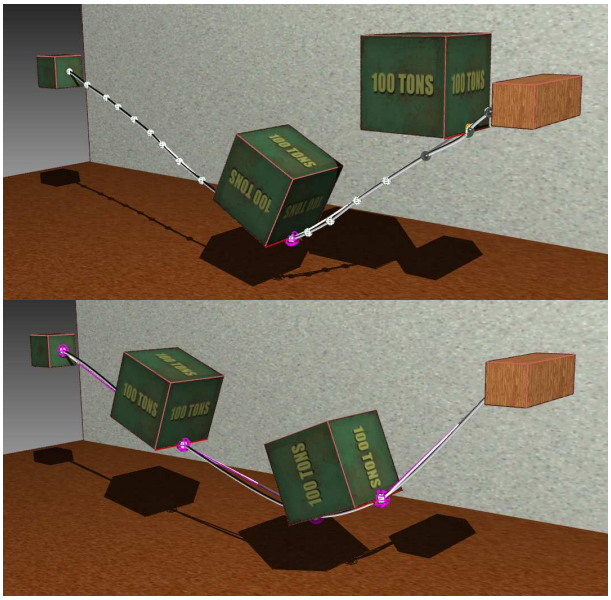

Fig. 1: *Demonstration example of hybrid, multiresolution wire. Heavy boxes are dropped on a wire. White nodes are massive. Purple nodes are massless frictional contact nodes. The wire has low tension and high resolution in the top figure when one of the loads comes into contact, producing smooth visuals and undulations. The wire is under very high tension in the bottom figure, supporting both heavy blocks. The resolution drops dramatically to maintain stability and the mass of the wire is concentrated on as few points as possible. This also corresponds to correct visuals, which are further improved by spline interpolations to produce the smooth white curve.*

B. Our contribution

We present a new wire model designed to meet the requirements for interactive visual simulation listed previously. This we coin the hybrid, multiresolution (HMR) model. The key idea is to combine the quasistatic *massless cable* approach with the multibody chain (or lumped mass) approach, extended to include dynamical contacts, and use of adaptive multiresolution to keep the computational cost at a minimum and guarantee numerical stability at high tension while allowing slacking at low tension. Sections composed of *massless* contact nodes are used to wrap a wire around geometries. These massless nodes are subject to dry friction meaning they can either stick to a given location on a body or slide along the edges of the geometry. The stick-slip transition is determined from the local pressure at each node. These nodes are removed when they slide out of range along an edge or when geometric analysis determines they are not needed. If the straight line between two given nodes does not touch any geometry, all intermediate massless nodes can be removed. If the straight line between two nodes on the wire collides with a geometry, one or several massless nodes are inserted on the edges of the geometry and the wire is re-routed along these nodes. The method is illustrated in Fig. 1.

Using massless instead of lumped mass nodes to model contacts between the wires and the geometry, it is possible to have a coarse resolution on free segments. Placing the massless nodes on the edges of the geometric models prevents penetration and wildly fluctuation contact forces that can be produced by the lumped nodes since these can touch anywhere, and since contacts might be detected after the fact with deep penetration. The potential for creating many massless nodes, which happens when a geometry is finely tessellated, is good for lashing and lassoing but it can have an impact on the performance. The latter is kept moderate by computing friction forces in *post facto* analysis which corresponds to a simple projection of computed forces into the feasible domain. It should be noted that the contact between a massless wire and other bodies (extended or points) is a different problem from dry frictional contacts between two rigid bodies. Firstly, in the massless wire case, there are in general more than two bodies interconnected by contacting wire. Secondly, the friction problem is inherently anisotropic, divided into friction *along* edges and *across* edges. Thirdly, stick and slip transitions should not only affect the connected massive bodies but also the motion of the quasistatic wire. Altogether, little theory from conventional rigid body frictional contacts can be reused.

The successful combination of adaptive resolution and massless contacting wire segments is essential for the results we presents that significantly expands the ranges of applications of wires in computer graphics animations based on physics simulation. This work include also analysis of scaling of the computational performance and numerical robustness in

comparison with the alternative of using the multibody chain approach, where the contacts are carried directly by the mass elements.

II. Hybrid, multiresolution wire

The HMR model combines lumped mass particles connected with distance constraints, and massless frictional nodes inserted wherever the wire comes in contact with other geometries. The mass nodes are created and deleted dynamically based on local stability criteria and geometric computation of contact location. This combination provides for the modeling of slacking and tensed wires which can be roped around bodies. The massless nodes used in roping can stick and slip based on local criteria involving the tension and the normal forces using standard Coulomb friction models but requires much less computations than using massive nodes for contacts. The routing of a roping configuration is computed using a minimization principle involving all the massless nodes of a given wire on a given body. A more precise mathematical description of these elements is presented below in Sec. II-A. Time integration requires solving a mixed linear complementarity problem (MLCP). We chose to use a specific integrator based on variational discretization, constraint regularization and a block-sparse linear solver but the general results does not hinge on this choice. Any of the time-integration techniques that are common in computer graphics, whether they use direct or iterative solvers or apply impulse and projection techniques, should benefit from the presented wire model in terms of computational performance and robustness.

A. Multibody dynamics

Our model consists of lumped masses which are either point particles or rigid bodies, and kinematic constraints between these. The coordinates of these elements are agglomerated in the generalized vector q, generalized velocity $v = T(q)\dot{q}$, mass matrix M, and generalized force f. These are all block vectors and matrices in which each block corresponds to either a point particle or a rigid body. The matrix $T(q)$ is block diagonal with identity blocks for the point particles and 4×3 blocks for the quaternions so that $\dot{q}_i = T_{ii}(q_i)\omega_i$ as is standard and well-known. The coordinates are resolved in the global inertial frame. When needed for clarity, the coordinates of an element with index $i = 1, 2, \ldots, N$, will be written x_i, and similarly for the other quantities. We will not resolve the individual coordinates of the block vectors.

Holonomic scleronomic constraints on our multibody systems are written $g(q) = 0$ and these produces forces $G^T\lambda$ where $G = \partial g/\partial q$ is the Jacobian matrix, and λ is the corresponding Lagrange multiplier. We use the descriptor form of the multibody equations of motion which means both that we need to compute the Lagrange multipliers λ explicitly and that the mass matrix M is block diagonal. The constraint functions $g(q)$ and the Jacobian matrices G are also partitioned in blocks. The block corresponding to constraint j and body i is written G_{ji}, and block constraint $g_j(q)$ corresponds to the multiplier λ_j. One distinguishing feature of our models is that we do not only consider simple joints which are constraints between only two bodies but we also include constraints which link several bodies together, indefinitely many in fact. The multibody wire constraint described below (in Eqn. (12)) could be used to model a pearl necklace with any number of pearls for instance as well as a wire wound about a collection of sticks.

We also use non-holonomic constraints which we write $Av + w(t) = 0$ and which produce a force $A^T\alpha$, where α is another Lagrange multiplier. The constraints for the stick-slip transitions of dry frictional contacts are treated approximately, outside of the main constraint force. We essentially impose non penetration constraints at the velocity level $Nv \geq 0$ where N is the block matrix containing the contact normals, and a non-slip condition $Dv = 0$ where D is the block matrix of contact tangents. The Lagrange multipliers for these are $\nu \geq 0$, the normal force, and β, the tangential, dry friction force, respectively. We approximately impose $\|\beta_i\| \leq \mu\lambda_i$ during the computation of the constraint forces. In our implementation, we impose the complementarity conditions

$$\begin{aligned} 0 \leq \nu \perp Nv \geq 0 \\ 0 \leq \beta - \beta_{\text{min}} \perp (Dv)_+ \geq 0 \\ 0 \leq \beta_{\text{max}} - \beta \perp (Dv)_- \geq 0, \end{aligned} \tag{1}$$

where $(Dv)_+ = \max(0, Dv)$, and $(Dv)_- = \min(0, Dv)$, i.e., the positive and negative parts of Dv. This makes Eqn. (1) a box complementarity condition. The values of β_{min} and β_{max} are adjusted dynamically. Details of this formulation differ according to the choice of multibody integrator [14] but are not essential to the HMR model described here.

The Newton-Euler equations of motion together with the holonomic and non-holonomic constraints form a set of differential algebraic equations (DAE). There are several alternatives to numerical time-integration of these. Many popular methods in computer graphics rely on a combinations of Verlet integration and Gauss-Seidel or conjugate-gradient iterative solvers for the Lagrange multipliers. Some of the current technique skip the explicit computation of the Lagrange multipliers and simply work directly on velocities and positions to force pairwise constraint satisfaction, e.g., [15]. These are often called impulse methods but the main difference with descriptor form is that the Lagrange multipliers are not stored but accumulated directly in the velocity change. Another method [14] is to maintain the matrix form and solve the MLCP with sparse matrices. We follow this latter approach but solve for the non-holonomic constraints iteratively post-facto. The hybrid multiresolution technique outlined in this paper should apply for the previously listed solver approaches as well.

For numerical time integration of the multibody system we use the SPOOK stepper introduced in [22]. This is a variational integrator based on Verlet discretization and constraint regularization using energy potentials that are squares of the constraints, i.e, $W = (1/2)g^T\varepsilon^{-1}g$. The resulting stepping scheme $(q_n, v_n) \rightarrow (q_{n+1}, v_{n+1})$, with time-index n and fixed step-size $t_{n+1} - t_n = h$, is efficient, robust at large time steps and allows for physical modeling of the response to constraint violation in term of viscoelastic properties. The regularization may be set infinitely stiff. After discretization and linearization

of the constrained equations of motion and constraints, we end up with a numerical model that involves solving a mixed linear complementarity problem (MLCP) [23] for each integration time step:

$$q_{n+1} = q_n + h\dot{q}_{n+1} \tag{2}$$

$$(\dot{q}_{n+1}, \lambda_{n+1}) = \texttt{solveMLCP}(H, b, l, u) \tag{3}$$

with the MLCP being

$$Hz + b = w_+ - w_- \tag{4}$$

$$0 \le z - l \perp w_+ \ge 0 \tag{5}$$

$$0 \le u - z \perp w_- \ge 0 \tag{6}$$

with

$$H = \begin{bmatrix} M & -G(q_n)^T \\ G(q_n) & \Sigma \end{bmatrix}, \tag{7}$$

$$z = \begin{bmatrix} T(q_n)\dot{q}_{n+1} \\ \lambda_{n+1} \end{bmatrix}, \quad b = \begin{bmatrix} -MT(q_n)\dot{q}_n - hF_n \\ -\frac{4}{h}\Upsilon g_n + \Upsilon G(q_n)\dot{q}_n \end{bmatrix}. \tag{8}$$

The vector z is the solution of the MLCP within the upper and lower limits u and l for a given vector b and slack variable w_+, w_- discarded once the solution is computed. The inequalities and orthogonality should be understood component wise. The matrices Σ and Υ are diagonal with regularization parameters according to

$$\Sigma = 4h^{-2}\,\mathrm{diag}\left[\tfrac{\varepsilon_1}{1+4\gamma_1/h}, \tfrac{\varepsilon_2}{1+4\gamma_2/h}, \ldots\right] \tag{9}$$

$$\Upsilon = \mathrm{diag}\left[\tfrac{1}{1+4\gamma_1/h}, \tfrac{1}{1+4\gamma_2/h}, \ldots\right]. \tag{10}$$

The regularization parameter ε can be directly related to conventional material parameters for elasticity, see Sec. II-B below. The term γ/h is a constraint stabilization parameter and correlates to the number of time steps for a constraint violation to be reduced by a factor of $1/2$. It is straightforward to introduce also velocity constraints based on Rayleigh dissipation functions. This can be used to model internal viscous damping.

Note also that one can reformulate the MLCP using only the Schur complement matrix

$$S_\epsilon = GM^{-1}G^T + \Sigma, \tag{11}$$

which is more common. Nevertheless, it is more advantageous to use the sparse matrix H of Eqn. (7) when using a good direct sparse solver since S_ϵ is always more dense than H. We justify our choice in the performance graph Fig. 8.

B. The N-body wire constraint

The HMR wire model consists of a chain of N_l massive nodes, either point particles or rigid bodies, connected pairwise via massless segments of length $L_j, j = 1, 2, \ldots, N_m = N_l - 1$. At any given time, each massless segment consists of N_j nodes at location p_k, connected with $N_j - 1$ subsegments of length $l_k = \|p_{k+1} - p_k\|$, $k = 1, 2, \ldots, N_j - 1$. The extreme nodes $k = 1$ and $k = N_j$ are massive whilst the intermediate ones are either contact or eye nodes. The number and location the massless segments and the nodes may change at each step according to the procedure described in Sec. II-C and Sec. II-D. Each node k is instantaneously fixed to a single massive body $i = b_j(k)$ which means that $\dot{p}_k = v_i + \omega_i \times d_i$, where $d_i = p_k - x_i$ for a rigid body, and $\dot{p}_k = v_i$ for a point particle. The body $b_j(k)$ is either one of the massive nodes of the wire or some other dynamic or static body in the simulation.

An example is illustrated in Fig. 2 in which one single massless segment connects two massive nodes at p_1 and p_4, via two intermediate contact or eye nodes at locations p_2 and p_3, each attached to a different bodies. There is no real distinction between eye and contact nodes except that the former are persistent between steps, i.e., they are linked to one and the same body and have fixed $\bar{d}_k$ in the body frame.

The constraint we wish to impose on each segment j is the preservation of the total length

$$g_j = \sum_{k=1}^{N_j-1} l_k - L_j = \sum_{k=1}^{N_j-1} \|p_{k+1} - p_k\| - L_j. \tag{12}$$

This reduces to the familiar distance constraint between two bodies for the case when there are no intermediate nodes. Since only the total length is preserved, each sub-segment length $l_k \ge 0$ may vary in time. This means in particular that contact and eye nodes can slide along the wire, like beads on a thread. Massless nodes can be added or deleted dynamically. Figures 6 illustrate the situation. The complete constraint for a given wire is the aggregate of the constraint on each segment $g = [g_1, g_2, \ldots, g_{N_m}]$, producing a force $G_j^T\lambda$ on the bodies carrying the the massless nodes. In the present case, the multiplier λ_j is the tension in the massless wire segment j. The constraint defined by Eqn. (12) is one dimensional and it contains as many nonzero blocks as the number of bodies interacting with the segment. The Jacobian for each massless segment become

$$G_j = \sum_{k=2}^{N_j-1} G_j^{(k)} + G_j^{(1)} + G_j^{(N_j)}, \tag{13}$$

with

$$G_j^{(k)} = \begin{bmatrix} 0 & 0 & \ldots & G_{jb(k)} & 0 & 0 & \ldots \end{bmatrix}. \tag{14}$$

Jacobian $G_j^{(k)}$ has a single row and as many columns as there are degrees of freedom in the system. The position of the nonzero block $G_{jb(k)}$ is that of body $b(k)$. That block evaluates to

$$G_{jb(k)} = \begin{bmatrix} (\hat{l}_{k+1} - \hat{l}_k)^T & -(\hat{l}_{k+1} - \hat{l}_k) \times d_k)^T \end{bmatrix} \tag{15}$$

for $2 \le k \le N_j$, and

$$G_{j1} = \begin{bmatrix} -\hat{l}_1^T & (\hat{l}_1 \times d_1)^T \end{bmatrix} \tag{16}$$

$$G_{jN_j} = \begin{bmatrix} \hat{l}_{N_j}^T & -(\hat{l}_{N_j} \times d_{N_j})^T \end{bmatrix} \tag{17}$$

at the extremities. For bodies that are of particle geometry there are no $\hat{l} \times d$ block components since particles have no rotational degrees of freedom. Observe that the Jacobian matrix G_j is very compact and has dimension $1 \times 6N$, if all bodies are rigid bodies.

The SPOOK stepper allows for physics based constraint regularization. We introduce stretch and bend viscoelasticity based on conventional material. As was shown in [18]

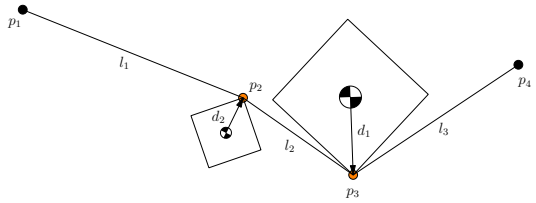

Fig. 2: *Schematics of the N-body constraint connecting two mass nodes (black) via intermediate contact nodes (yellow).*

and [19] the mapping between regularization parameters for stretching and bending deformations, cable dimensions and the Young's modulus Y are $\varepsilon_{\text{stretch}} = (l_a + l_b)/4YA$ and $\varepsilon_{\text{bend}} = (l_a + l_b)/4Y_A$, where A is the wire cross-section area and I_A is the area moment of inertia along the central axis normalized by mass. For circular cross-sections $I_A = \pi r^4/4$. The bend elasticity requires complementing the model with angular constraints $g_{\text{ang}} = \arctan(|\hat{l}_k \times \hat{l}_{k+1}|/\hat{l}_k \cdot \hat{l}_{k+1})$. The present model can easily be extended to include also constraints and elasticity for wire torsion [19]. If desired, the material parameters may be set arbitrarily stiff or soft to simulate unnatural materials as well.

C. The dynamics of massless contact nodes

Contacts between a wire and a geometry, attached either to a massive or a static body, generate massless node on the edges of the model. The massive wire nodes never touch the models directly. The wire can therefore have as sparse a distribution of mass nodes as needed to meet the stability criteria and still have as many contacts nodes as required by the resolution of the geometric models. See Fig. 3 for an example.

In our implementation, the wire segments are represented by thin cylinders which are tested against the other models applying broad and narrow phases as customary. For positive tests, the set of edges of the tessellation of the model, $\mathcal{E}$, are then tested against the thin cylinder representing the wire. The edge e_k closest to an existing node on the wire is then selected and a massless node k is added to the corresponding set $\mathcal{C}_j$. The new node is positioned at location p_k on the edge which minimizes the distance to both nearest neighboring nodes, which may be massive or not. In other words, p_k minimizes the change in constraint violation so that

$$p_k = \underset{p_k \in e_k}{\operatorname{argmin}} (g_j)\,. \tag{18}$$

The complete node management procedure starts with removal of existing nodes which have inward pointing contact force or have reached a vertex. The edges in stick friction are kept at their location on their edge. The edge-wire collision detection is then applied iteratively, creating nodes where there is penetration, and temporarily removing nodes that have outward directed contact force or have reached an edge. The latter might be moved to an adjacent edge during the iterations. This is repeated until a *detaching* state is found, i.e., when the wire lies entirely on or outside the surface of the model, and there is no adhesive force at any of the contact locations.

1) Frictionless contacts: Contact forces and torques corresponding to $G^T\lambda$ are computed to satisfy the wire constraint $0 = g_j$ as accurately as possible at the end of the time step. The Jacobian matrix is evaluated at the beginning of the time step, and the multiplier vector λ is found by solving the MLCP of Eqn. (4)–(7). The MLCP reduces to a linear system (4) if there is no complementarity condition such as stick slip transitions. One can also solve the linear system neglecting the complementarity conditions and then project the result on the given bounds. The force on body $b(k)$ resulting from contact node k of the wire segment j is

$$F_{jb(k)} = \begin{bmatrix} f_{jb(k)}^T & \tau_{jb(k)}^T \end{bmatrix}^T = G_{jb(k)}^T \lambda_j, \tag{19}$$

where $G_{jb(k)}$ is given by Eqn. (15). The explicit form of the node contact force is needed both for identifying detachment and for computing friction forces. The edge direction is denoted $\mathbf{t}$ and the edge normal, $\mathbf{n}$, is the average of the normals of the adjacent surfaces. The normal and tangential forces at that edge are then

$$N_k = \mathbf{n}^T f_{jb(k)}, \text{ and } T_k = \mathbf{t}^T f_{jb(k)}, \tag{20}$$

respectively. Detachment occurs if $N_k \geq 0$, i.e., when the force points outward from the geometry. In the absence of friction, the wire should not produce any forces tangential to the edge and be free to slide along the edge. The condition for this is $T_k = 0$. This is accomplished by continuously updating the node positions p_k according to Eqn. (18). We solve this optimization problem each time step by Gauss-Seidel iterations over the contact list $\mathcal{C}$. Two iterations in opposite direction have proved sufficient in practice, since the wire configuration is close to optimal from the last time step. By this operation each node is shifted some distance Δp_k along the edge to a new position $p_k + \Delta p_k$ which minimizes the segment length, see Fig. 4. Although the wire is stiff, it is in general slightly stretched by gravity or contact forces. If the node update finds that Δp_k compresses the wire the contact node is released and a mass node is introduced instead.

2) Frictional contacts: We distinguish between *stick (or static) friction* and *slide (or kinetic) friction*. For stiction friction, the wire should neither slide *along* the edge nor *across* the edge. This means that the node position p_k is fixed with respect the center of mass of body $b(k)$ between time steps. This also means that the distance between that node and neighboring massive wire nodes is constant, implying an additional constraint $\bar{g}_j = 0$. The frictional force produced by this constraint is $\bar{f}_{b(k)} = \bar{G}_{jb(k)}\bar{\lambda}_j$. When the stick friction force exceeds the threshold

$$|\bar{f}_{b(k)}| \leq \mu |N_{b(k)}| \tag{21}$$

the stick friction vanishes and is replaced by slide friction. The effect of slide friction is a force on the contacting objects proportional to the normal force and tangential to the edge, i.e., $\bar{f}_k = \pm\mu|N_k|\mathbf{t}$. Since the wire contact node is massless we cannot directly apply forces to it. Instead we model the slide friction by reducing the computed slide distance Δp_k by a factor $1 - \mu$, i.e.,

$$p_k \rightarrow p_k + (1 - \mu)\Delta p_k. \tag{22}$$

In effect, this reduces the sliding velocity of a wire along an edge by a factor $(1-\mu)$.

This form of post facto computation amounts to a projection of the constraint force on the surffice of the Coulomb friction cones one equation at a time. This is the same as performing a single projected Gauss-Seidel iteration to solve the contact forces. Note also that μ is a *pseudo* friction coefficient since friction coefficients can be larger than one. We ignore this since we are looking at the qualitative aspect of stick and slide friction. A stick mode is absolutely necessary for lashing and grabbing and Eqn. (22) can produce that for $\mu = 1$. Likewise, slide friction should cause a reduced acceleration. Because of the many constraints which oppose each other, only the net balance of forces can be certain, i.e., only the sum of the constraint forces is correct. Basing a friction model on any one of these forces is bound to be approximate.

Note also that there are anomalies at zero friction. This is because nodes are never considered frictionless a priori. If μ is very small, this means an anomalous stick-slip transition at each step which has no relation to the real situation. These effects do appear in our results as seen in Figure 13.

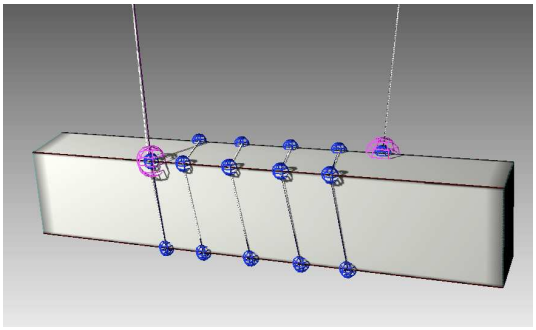

Fig. 3: *Image of massless wire wound about a rigid block. The wire is in the state of minimal resolution. All nodes are massless contact nodes living on the edges of the colliding geometry. The larger purple spheres indicate frictional contacts.*

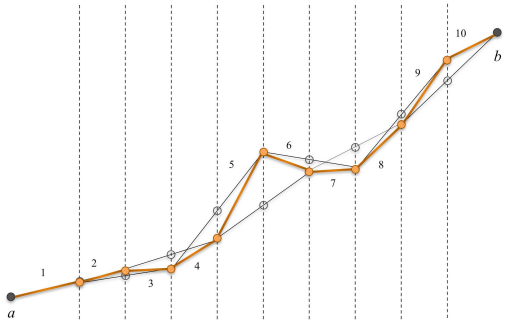

Fig. 4: *Illustration of the update procedure for contacts on the edges of a block winded up in a wire as in Fig. 3. The end-nodes a and b are the wire end nodes (attached to the world or other objects). Yellow nodes are current contact nodes living on the edges of the block. The open circles are node positions that minimize the length of the segment. The wire will be updated to these positions if there is no friction.*

For the adaptive HMR model with frictional contacts, Eqn. (21) give complementarity conditions (5)–(6) for wire segment Lagrange multipliers λ_j and $\bar{\lambda}_j$ with the upper and lower bounds

$$u = l = \frac{\mu|N|}{\sqrt{\bar{G}_{jk}^T \bar{G}_{jk}}}. \tag{23}$$

D. Adaptive multiresolution

Adaptive spatial resolution helps striking a good balance between computational time, visual appearance, stability, and realistic motion. The geometric configuration, the view-point of the observer, and the state of motion all contribute to determine an adequate level of detail. A good model should economize on computations which neither contribute to the visuals or to the accuracy. A wire under high tension is well approximated by a straight segment for instance.

Resolution is also intimately linked to numerical stability and physical realism. Consider a single point mass m_b along a wire connected by segments of length l_a and l_c to its nearest neighbors, which necessarily belong to different massless segments. These have tension f_a and f_c, respectively. The resulting transversal force f_t for a transversal displacement Δx satisfies the linear relation

$$f_t = \left(\frac{f_a}{l_a} + \frac{f_c}{l_c}\right)\Delta x, \tag{24}$$

producing the oscillation frequency $\omega^2 = 2f(l_a^{-1} + l_c^{-1})/m_b$. The stability criterion for the Verlet integrator which we use in our implementation is $h^2\omega^2 < 4$. This translates to an upper bound on the allowed tension

$$f_t < f_{\text{crit}} \equiv \min(l_a, l_c)\frac{m_b}{4h^2} \tag{25}$$

A consequence of Eqn. (25) is that for a wire of length L and mass M, a uniform discretization in N segments leads to $l_a = l_c = L/N$ and $m_b = m = M/N$, and so

$$f_{\text{crit}} = \frac{LM}{4N^2h^2}, \text{ for regular discretization.} \tag{26}$$

This shows clearly how limiting the homogeneous and fixed discretization can be. For given tension, the step size must decrease linearly with increased resolution. At fixed resolution, the time step must be reduced quadratically with respect to the applied tension. Increasing the load on a wire by a factor of ten requires a reduction in time step by a factor of a hundred.

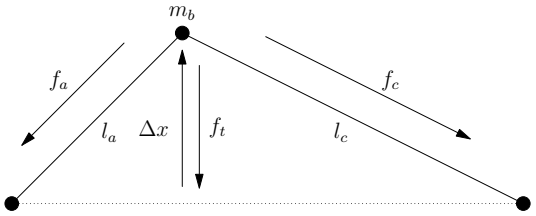

Fig. 5: *Longitudinal tension causes transversal forces on the massive nodes to restore a straight line.*

For our massless segments, Eqn. (25) restricts $f_j = G_j^T \lambda_j \ll f_{\text{crit}}$. When fewer nodes are used, both $\min(l_a, l_c)$ and m_b increase linearly which means that the maximum allowed tension increases quadratically with coarsening operations. This quadratic relation makes it easy to quickly reach the stability region without too much computation.

The heart of multiresolution is the use of Eqn. (25) locally, and quasistatically. The coarsening and refinement procedure starts with testing each massive node against the criterion in Eqn. (25). The lengths l_a and l_c are measured relative to the nearest neighbors, massless or otherwise. Negative results are first considered and problematic nodes are removed. The mass of these is distributed to the closest massive neighbors in proportion to the respective lengths l_a and l_c. This is repeated iteratively until all nodes are well inside the stability region. The second phase considers the massive nodes m_b which have local oscillation frequency below a given threshold of f_{crit}. The mass of these is distributed proportionally among new nodes positioned uniformly on the segments l_a and l_c. This is done iteratively until either a maximum resolution or the stability threshold are reached.

This procedure actually makes a wire flow smoothly over contact nodes without any modification. As the critical frequency decreases linearly with the distance to the next contact location, mass node moving toward a contact will eventually be considered for removal and part of its mass added to the first node moving away from the same. Since both the removal criteria and the mass redistribution are linear in the distances to and from the contact location, the mass flow is linear in the relative speed between the wire and the contact point.

The adaptive multiresolution technique at work is illustrated in Fig. 6, showing a box dropped onto a suspended wire, insertion of contact nodes, mass node coarsening to avoid numerical instability and refinement to regain resolved dynamics.

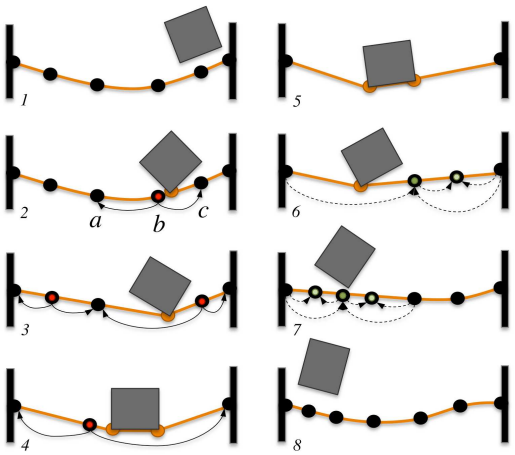

Fig. 6: *Illustration of the hybrid, multiresolution wire model with a heavy box dropped onto it. The wire consists of mass nodes, the black circles, connected by massless segments, the yellow lines. Contacts are carried by massless contact nodes, the yellow circles, instead of the massive nodes. Resolution is adapted for avoiding numerical instability at high tension.*

We use the following *coarsening transition rules* for merging mass b with neighboring mass nodes a and c at wire distance l_a and l_c from b, respectively:

$$m_a \rightarrow m_a + \Delta_c m_b \tag{27}$$
$$m_c \rightarrow m_c + \Delta_a m_b \tag{28}$$
$$v_a \rightarrow \left(\frac{m_a}{m_a+\Delta_c m_b}\right) v_a + \left(\frac{\Delta_c m_b}{m_a+\Delta_c m_b}\right) v_b \tag{29}$$
$$v_c \rightarrow \left(\frac{m_c}{m_c+\Delta_a m_b}\right) v_c + \left(\frac{\Delta_a m_b}{m_a+\Delta_a m_b}\right) v_b \tag{30}$$

where $\Delta_a = l_a/(l_a + l_c)$ and $\Delta_c = l_c/(l_a + l_c)$, which are weight factors managing that mass and momentum is transferred mostly to the nearest mass node. The *refinement transition rules* for splitting two mass nodes a and c, and create one new mass node b at the center of mass position of a and c, thus splitting the segment in two, of lengths l_a and l_c from b is

$$m_a \rightarrow m_a - \Delta_a m_b \tag{31}$$
$$m_b \rightarrow \tfrac{1}{2}\min(m_a, m_c) \tag{32}$$
$$m_c \rightarrow m_c - \Delta_c m_b \tag{33}$$
$$v_a \rightarrow v_a \tag{34}$$
$$v_b \rightarrow (m_a - m_b)v_a + (m_c - m_b)v_c \tag{35}$$
$$v_c \rightarrow v_c \tag{36}$$

The transition rules Eqn. (27)–(30) and Eqn. (31)–(36) are constructed to preserve the physical invariants as much as possible. In particular, the transition rules preserve the total mass and rest-length of the wire, the total momentum in the system and do not add energy to the simulation.

The barycentric refinement used here, can cause imbalance in the bending energy as previously reported [5]. This effect is negligible in comparison to stretching energy in our applications, which is preserved. Clearly, the two methods could be combined using a criterion to include curvature energy when it is significant and stability allows.

E. Algorithm

The complete HRM method is described in Algorithm 1. The constraint accumulation in step 6 : may also include all other constraints in the systems such as joints or contacts between rigid bodies. Because many of our examples involve large mass ratios, we use a direct, sparse matrix factorizer

Algorithm 1 Hybrid, multiresolution wire algorithm

1: system initialization $(q, \dot{q}, g, M)$
2: **while** running **do**
3: accumulate external forces and user interaction
4: collision detection $\rightarrow$ add new wire contacts to $\mathcal{C}$
5: adapt wire resolution $\rightarrow$ add/remove mass nodes
6: accumulate constraints $(g, \bar{g})$
7: compute Jacobians $(G, \bar{G})$
8: build the data (H, x, l, u) in Eqn. (8), (7), (23)
9: `solveMLCP(`H, x, l, u`)` $\rightarrow (\dot{q}_{n+1}, \lambda_{n+1})$
10: update body positions $q_{n+1} = q_{n+1} + h\dot{q}_{n+1}$
11: update no-sticking nodes in $\mathcal{C}$ (slide or detach)
12: **end while**

to solve the linear system in (4). The overall procedure to solve the MLCP is a form of Newton's method [22]. We have successfully used the sequential version of SuperLU [25] with defaults parameters. Both speed and scalability have proved sufficient. For our examples at least, the computational time grew linearly with the number of bodies.

III. Results

We now present results of numerical experiments of the HMR wire model presented in section II. The experiments are designed to evaluate computational performance, numerical stability, and the quality of contact configurations. Comparisons are made with a conventional multibody chain (MBC). The MBC model consists of massive nodes linked by simple distance constraints equally distributed along the wire. In comparative tests, the global physical parameters such as total mass and elasticity are identical in both models. All simulations share the same fixed time step $h = 1/60\ s$ and uniform gravitational acceleration $g_{\text{acc}} = 9.81\ m/s^2$. All objects have similar length scales in the range of 1–50 m. All tests were implemented using the AgX Multiphysics [26] library with SuperLU [25] as the sparse linear solver. Experiments were performed on a desktop computer with Intel(R) Core(TM) i7 950 , 3.07 GHz, 6 GB RAM and on a Windows 7 64-bit system, and all programs were single threaded.

A. Performance

The first series of tests measure performance and scalability of the HMR method and of step 3-11 of Algorithm 1 to be precise. This is done for the three examples appearing in Fig. 7. The linear and network configurations at the top and lower left corner of the figure, respectively, test the performance and scalability of the core linear solver. These two configurations were chosen since they represent best and worse case scenarios for a direct solver. The large number of closed kinematic loops in the network scenario would produce a full matrix if we used the Schur complement matrix (11), and the performance would scale as $O(N^3)$. The sparse formulation (7) could also lead to bad performance unless a good direct solver such as SuperLU is used. The tests were performed on both HMR and MBC producing results shown in Fig. 8 and clearly indicate linear complexity. The yellow dots represent minimal resolution which the HMR model automatically adapts to when under tension, and the lines correspond to increased resolution. These curves establish the basic computational cost using a direct solver, which is between 0.01 and 0.03 milliseconds per node. Other direct linear solvers may perform better or worse, but they should only introduce a bias, without affecting the overall linear complexity. The spurious jumps in the graph are due to memory storage and caching effects.

The example illustrated in Fig. 10 also shows the setup for the performance test wire contacting with a geometry. The load is chosen such that the HMR wire adapts to minimal resolution. The number of contact nodes then depends on the geometry mesh. We choose parameters so that the HMR and MBC models both contain Nnodes. At equilibrium, HMR needs two massive node where the wire leaves the surface of

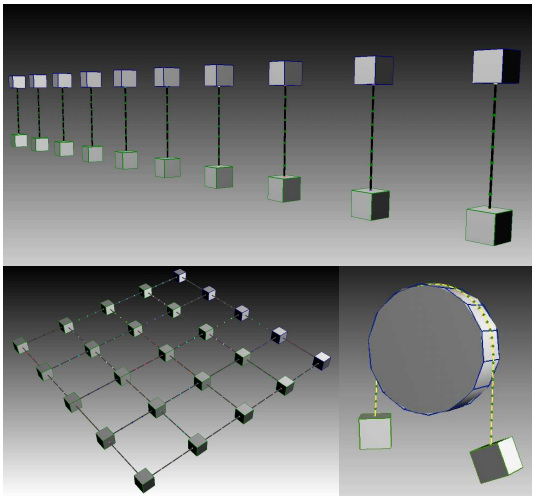

Fig. 7: *Test systems for performance measurements. The test systems are chain, net and suspension over a static geometry.*

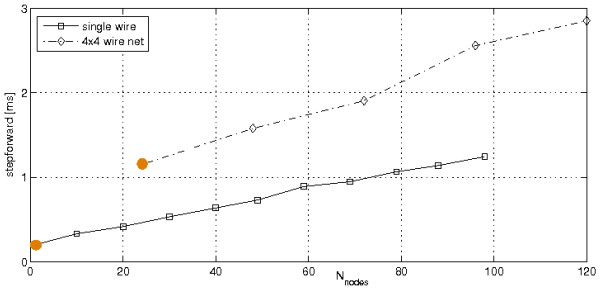

Fig. 8: *The computational performance of wires in chain and net topology at different resolutions. Yellow marks minimal resolution.*

the cylinder, connecting to the loads, two massless frictional nodes at the same locations, and $N - 4$ massless contact nodes lie on the cylinder itself. The MBC wire contains N massive nodes in total. The comparison is meaningful since it measures the computational cost of a given spatial resolution. The performance curves are shown in Fig. 9. The MBC scales linearly as it should, but the HMR reaches a near plateau. This is because there are many fewer constraints in the HMR model since all the contact nodes are actually on the same massless wire segment. The two frictional nodes bring a single equation each, and so do the final segments attached to the loads. An example of the distribution of the contact nodes for the HMR model is shown in Fig. 10.

At equilibrium, the HMR model settles with one constraint preserving the total length and two frictional constraints for the first contact node on each side. The matrix H in Eqn. (4) is therefore 15×15, since there are two bodies with 6 equations each, and 3 constraints with one equation each. For a MBC wire with N mass elements, the H-matrix has dimension $(12+4N-1) \times (12+4N-1)$, omitting friction. There are 12 rows for the 2 rigid bodies, $N-1$ distance constraints, and N spherical rigid bodies requiring $3N$ equations. There is a small cost of having more contact nodes in the HMR model but that is not part of the solver cost but of the preparation stage of

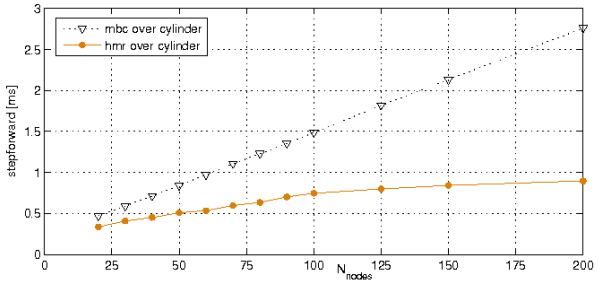

Fig. 9: *The computational performance of a multibody chain wire and a hybrid, multiresolution wire at minimum resolution in resting contact over a cylinder geometry of variable discretization.*

Algorithm 1, namely, steps 4 to 7. The computational cost of the MBC model is as before, namely, roughly $0.013ms$ per mass node. But for the HMR, each new contact costs roughly $0.003ms$.

B. Robustness at high tension

The numerical stability is assessed by hanging heavy loads at the ends of the wire. According to the theory resulting in the criterion of Eqn. (25), the MBC should quickly loose stability but HMR should remain stable for any realistic load. In Fig. 10, the loads have mass m_b and the wires both have mass m_w. These were both varied between 1 and 10^5 kg, and the cable resolution was varied from 1 to 30 segments. This represents the maximal resolution for the HMR model which distributes nearly all the nodes over the cylinder according to Algorithm 1 as explained before. As usual, we choose a fixed integration step of $1/60$s, corresponding to the requirements of our realtime applications. The results produced the stability matrix displayed in Fig. 11. The masses m_w and m_b form the xy axes and the resolution is indicated in the respective boxes. Boxes marked with a cross correspond to unstable configurations. These were identified as wild vibrations in the wire, unnatural elongation or by that the wire simply exploded. The threshold for instability was defined as constraint violations of the order of 5 %. The results obviously validate the theory. The HMR wire automatically adapts to a stable level of resolution. The MBC is only stable for a small range of node vs load mass on the diagonal, and it is nearly impossible to put enough nodes to smoothly fit the cylinder and keep good contacts.

When the load to wire ratio reaches $m_b \gtrsim 100m_w$, there are no stable configurations. This may not appear to be a bad limitation for offline computations since the time step could always be chosen small enough, gravity could be tuned, or the mass ratios could be tuned. Adjusting the time step leads to prohibitive computational cost, especially if one wants to have good contact resolution around the geometries. For comparison, consider a MBC simulation of the demonstration system in Fig. 14 with a $1\ kg$ wire $10\ m$ long wrapped about a $100\ kg$ block. For the MBC model to resolve the contacts this requires spatial resolution of at least $l = 0.01\ m$ which means wire elements of mass $m_b = 10^{-3}\ kg$. The wire tension for static support of the block is about $f = 1000\ N$ and according to Eqn. (25) the maximal time step for numerical stable simulation is $h < \sqrt{m_b l/4f} \sim 5 \times 10^{-5}\ s$. This is a factor 3×10^{-3} smaller than what is used in the demonstration of HMR and involves simulation of 1000 wire elements. In the case of using a HMR wire the sum of wire elements and contact nodes is well below 100. According to Fig. 9 this adds yet another factor 10 to the computational time for the MBC compared to the HMR wire. Applying adaptive resolution to the MBC reduces the number of wire elements but not the occurrence of small masses and computational speed will thus still be at least a factor 10^3 apart from the HMR. In a dynamic situation, e.g., when the wire unwinds with stick and slip events, the wire tension may peak at higher values and even smaller time steps may be required for the MBC wire simulation.

By contrast, the HMR model produces as many contacts as there are edges in the way, i.e., precisely what is needed to produce correct visuals corresponding to exact non penetration. The cost is essentially that of collision detection. Since the mass ratio corresponds directly to the condition number of matrix H in Eqn. (4), the stability is entirely related to the linear solver. In double precision, a direct solver can easily handle condition numbers of 10^{12} at least, according to numerical analysis. This is well above what is realized in any practical applications.

The exact stability domain for iterative solvers was not investigated.

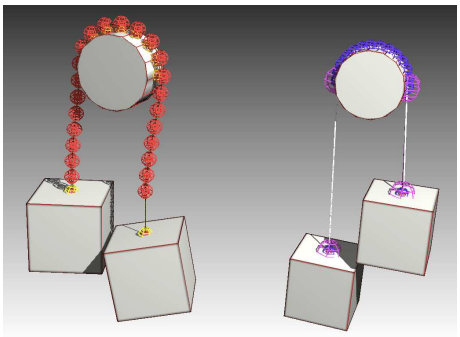

Fig. 10: *The system for testing numerical robustness. The conventional multibody chain on the left maintains contact with the cylinder through the rigid spheres shown in red. These are attached to each of the massive node in the chain. The hybrid multiresolution wire on the right maintains contact with the surface through massless nodes shown in blue.*

C. Frictional contact measurements

The simplified frictional contact model derived in Sec. II-C2 was tested against the Coulomb model for both stiction and sliding modes. This is done both for motion along an edge transversal to the wire, and over an edge in the longitudinal direction. The setups are illustrated in Fig. 12. Here, a wire with loads at both ends rests on a simple rectangular beam. Using the HMR model, this produces two contact and two frictional nodes. The top part illustrates the tests measuring friction along an edge by using equal loads with mass m_b

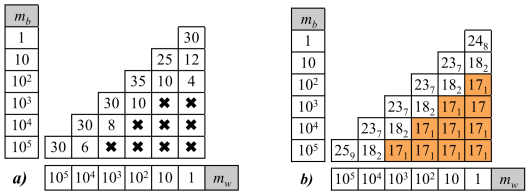

Fig. 11: *Numerical stability charts for wire mass m_w versus box mass m_b for the test system in Fig. 10. Chart a) displays the lowest level of resolution for a stable conventional multibody chain wire. Chart b) displays the resolution level to which the hybrid multiresolution wire adapts according to the rules described in Algorithm 1 to maintain stability.*

and inclining the beam by an angle θ measured from the horizontal. The bottom part contains the setup used to test for sliding across edges by using unbalanced loads of mass $m_{\mathrm{b}}^{(1)} \leq m_{\mathrm{b}}^{(2)}$ on a level beam. Both examples correspond directly to the Coulomb model in which the frictional force f_T builds up to resists sliding so $f_T \leq \mu \|f_N\|$, where $\mu > 0$ is the friction coefficient, and f_N is the normal force at the contact. Transversal and longitudinal cases are studied independently since we use a different models for each.

For the transversal friction test, the normal and tangential forces at each contact node are $f_N = m_{\mathrm{b}} g \cos(\theta)$ and $f_t = m_{\mathrm{b}} g \sin(\theta)$, respectively. We ran simulations for masses $m_{\mathrm{b}} \in [10, 1000]$ kg, angles $\theta \in [5, 30]$ degrees, and friction coefficient $\mu \in [0, 1]$. We measured the acceleration of loads projected along the contacting edges. This is zero for the stiction case and should be constant for the sliding case. Representative results for $\theta = 30°$ are displayed in Fig. 13. The net tangential force is $-mg(\sin(\theta) - \mu\cos(\theta))$, so the acceleration should drop linearly from $-g\sin(\theta) = -g/2 = -4.9m/s^{(2)}$ to 0 according to $a = (g\sin(\theta))(1 - \mu\sec(\theta))$, reaching stick friction at $\tan(\theta) = \mu \approx 0.58$. Apart from variations of the order 10 % the acceleration decreases monotonically but stick is reached only at $\mu = 1.0$. The spurious variations depends both on the non-ideal setup with load oscillations and of the artificial stick-slip transitions that occurs because of the *post facto* approximation and the simplifications made in deriving Eqn. (22), as discussed in Sec. II-C2. The artificial stick-slip transitions are not visible to the naked eye but shows up as numerical friction in the transversal direction and is present also in the case of $\mu = 0$.

The longitudinal friction test uses masses $m_{\mathrm{b}}^{(1)} = r m_{\mathrm{b}}^{(2)}$, with $r = 0.5$, and $m_{\mathrm{b}} \in [10, 1000]$ kg. We measured the vertical acceleration of the boxes to compute the frictional force. In zero friction, the tension in the cable is uniform and the test reduces to the Atwood machine. In this case, the tension is uniform along the wire and the acceleration of the bodies are equal and opposite with $a = g(1-r)/(1+r) = g/3 \approx 3.3 \quad m/s^2$ for our choice $r = 0.5$. The tension itself is $f = 2rm_{\mathrm{b}}/(1+r)$. The pressure at the contact nodes is $\sqrt{2}f$ because of the 90° turn. Our slide friction model should simply decrease this acceleration linearly with μ but this is not exactly what is observed in Fig. 13. This is most likely because of the *post facto* approximation and the simplifications made in deriving Eqn. (22).

In both cases, the friction model can produce pure stiction which is needed for stable grips, and produces the correct dynamics in zero friction. The qualitative aspects of the curves in Fig. 13 are correct in that net acceleration decreases nearly linearly with the friction coefficient, except near $\mu \approx 1$ which was chosen as a cutoff.

Fig. 12: *The systems for validating the friction model. Sliding along edges, top, and across edges, bottom.*

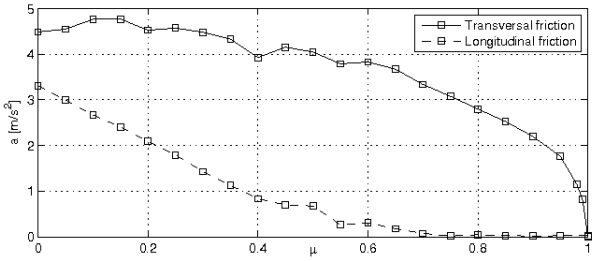

Fig. 13: *Measurements of the acceleration of the wire-box systems in Fig. 12 for different friction coefficients.*

IV. Demonstration Examples

The range of functionality of HMR model is illustrated with three cases. The first appears in Fig. 1 which prominently features stability and faithful contact resolution. The boxes really weigh 100 tons in this examples and the wire weighs only 50 Kg, a ratio of 4000 to 1 when both boxes are resting on the cables. The markers show clearly that the contacts are where they should be, not at arbitrary locations dictated by a uniform discretization. There is also no penetration whatsoever because the contact locations are put precisely on the surface. Slacking and tensing produce both correct visuals and more realistic rebounds, at least to the naked eye. The black lines are the massless wire segments. The white line is a spline interpolation. The criterion used to control the resolution in Eqn. (25) is very robust in practice because it aggressively

decimates light nodes. The second example shown in Fig. 14 displays the robustness of the contact resolution technique. There is no geometric penetration at all when the wire is wrapped and practically no slack in the first frame on the upper left hand panel. The large number of actual contact nodes produces a very stable grip. As the box is dropped, the wire slides along the surface and contact nodes are removed as needed. When the box finally detaches, slack is introduced with higher resolution massive nodes. The cable finally swings and whips. In this case, the block and wire weigh 100 kg and 1 kg, respectively. Third example in Fig. 15 illustrates the versatility and flexibility of the technique. Here, a gantry crane moving on horizontal rails is designed to pick up and deliver loads at opposite ends of the scene, moving over obstacles. The loading mechanism consists of pulleys, rolling drums, counterweights etc. This design lets the wire slide through the gripper eyes so that the gripper remains leveled despite a swinging load. This corresponds to a realistic application in which good agreement between experiment and simulation is needed. It is not clear whether such a scene could be realized at all using MBC models. Elasticity values for steel wires were used in the last two examples. In the first example the stiffness of wire was over exaggurated.

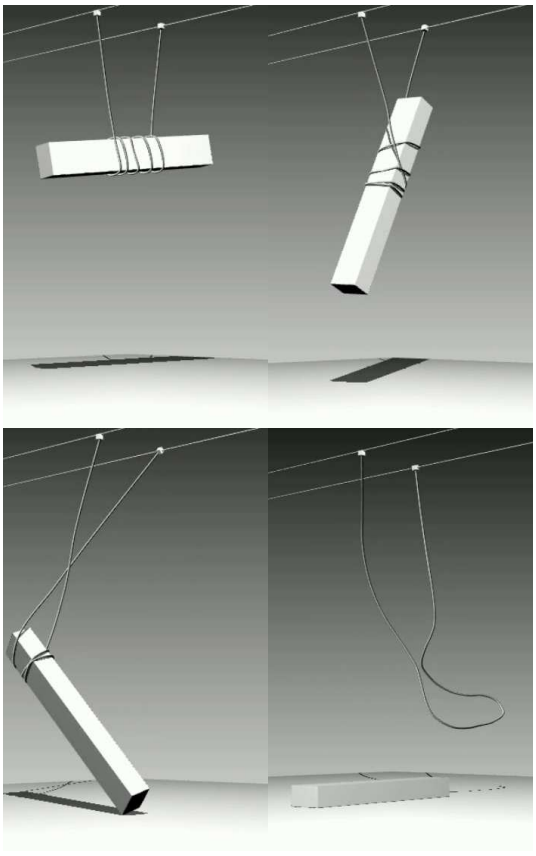

Fig. 14: *Demonstration example: wrapping a string about a body and letting it rewind under the pull of gravity.*

V. Summary and discussion

Nonuniform adaptive resolution based on local stability criteria provides a simple and robust technique for adding

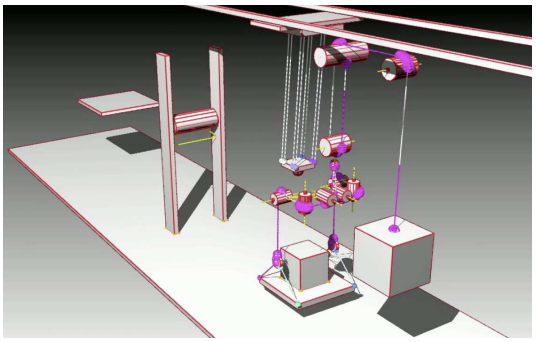

Fig. 15: *Demonstration example: a simple crane system with rope and pulleys.*

levels of details only where needed and when numerically safe. This improves graphics quality and decreases the computational time, both because the total number of equations is dramatically reduced and because the time step can be kept large. This can be adjusted to be fast enough for real-time context. Multiresolution techniques are not new and the can certainly be applied to other types of deformable bodies made of massive elements, something we plan to do in the near future.

The real novelty of the HMR model is the introduction of massless contact nodes in constraint based massless wire segments, together with a simplified dry friction model applied directly at these. This is a departure from basic multiresolution techniques which amounts to removing all the mass at certain vertices but keeping the constraints they impose on the rest of the system. An important example of this is dry frictional contacts which include non penetration constraints as well as restriction on forces and velocities.

By using contact nodes located on the edges and vertices of the models, the non penetration constraints are met exactly, and the wire follows contacting surface exactly. The combination of this geometric feature and a simple dry friction model produces stable contacts making it possible to wrap wires around objects for lifting, lashing, and lassoing, something that is nearly impossible to do with any speed and stability with MBC models. Indeed, it is possible to adaptively discretize MBCs, but unless the massive nodes are positioned explicitly, it is not possible to resolve the contacts at the edges of the geometries. In addition, a wire wrapped tightly around an object exhibits both high tension and large normal forces which is not a good recipe for stability.

Moving massive nodes over edges or past eye nodes is no simple matter in the MBC model, but is a fundamental feature of our HMR wire model. The HMR wire model can also include twist elasticity as shown in Ref. [19].

The model has limitations however. Self contacts are certainly possible between massive nodes at low tension using known methods [5]. But some form of contact nodes would be needed for high tension cases. This we leave for future developments. Another interesting direction for the future is to apply the HMR approach to other simulation techniques, such as *position based dynamics* with fast iterative solvers combined with constraint projection [17].

ACKNOWLEDGMENTS

This research was supported in part by VINNOVA/ProcessIT Innovations; the Swedish Foundation for Strategic Research (SSF) under the frame program grant SSF-A3 02:128; and by the Kempe foundations, grant JCK-2613. The authors wish to acknowledge Niklas Melin and other staff at Algoryx Simulations for help with programming and rendering.

REFERENCES

[1] D. K. Pai, "STRANDS: Interactive simulation of thin solids using cosserat models," *Computer Graphics Forum*, vol. 21, no. 3, pp. 347–352, 2002.
[2] S. Antman, *Nonlinear Problems of Elasticity (Applied Mathematical Sciences)*, 2nd ed. Springer, 2005.
[3] A. Nealen, M. Mueller, R. Keiser, E. Boxerman, and M. Carlson, "Physically based deformable models in computer graphics," *Computer Graphics Forum*, vol. 25, no. 4, pp. 809–836, 2006.
[4] M. Bergou, M. Wardetzky, S. Robinson, B. Audoly, and E. Grinspun, "Discrete elastic rods," *ACM Transactions on Graphics*, vol. 27, no. 3, pp. 63:1–63:12, Aug. 2008.
[5] J. Spillmann and M. Teschner, "An adaptive contact model for the robust simulation of knots," *Computer Graphics Forum*, vol. 27, no. 2, pp. 497–506, 2008.
[6] R. Gayle, M. Lin, and D. Manocha, "Adaptive dynamics with efficient contact handling for articulated robots," in *Proceedings of Robotics: Science and Systems*, Philadelphia, USA, August 2006.
[7] S. Redon, N. Galoppo, and M. C. Lin, "Adaptive dynamics of articulated bodies," in *SIGGRAPH '05: ACM SIGGRAPH 2005 Papers*. New York, NY, USA: ACM, 2005, pp. 936–945.
[8] M. Grégoire and E. Schömer, "Interactive simulation of one-dimensional flexible parts," *Comput. Aided Des.*, vol. 39, no. 8, pp. 694–707, 2007.
[9] D. Terzopoulos, J. Platt, A. Barr, and K. Fleischer, "Elastically deformable models," in *SIGGRAPH '87: Proceedings of the 14th annual conference on Computer graphics and interactive techniques*. New York, NY, USA: ACM, 1987, pp. 205–214.
[10] S. Hadap, "Oriented strands - dynamics of stiff multi-body system," in *2006 ACM SIGGRAPH / Eurographics Symposium on Computer Animation*, Sep. 2006, pp. 91–100.
[11] F. Bertails, B. Audoly, M.-P. Cani, B. Querleux, F. Leroy, and J.-L. Lévêque, "Super-helices for predicting the dynamics of natural hair," in *SIGGRAPH '06: ACM SIGGRAPH 2006 Papers*. New York, NY, USA: ACM, 2006, pp. 1180–1187.
[12] D. Baraff, "Analytical methods for dynamic simulation of non-penetrating rigid bodies," *SIGGRAPH Comput. Graph.*, vol. 23, no. 3, pp. 223–232, 1989.
[13] ——, "Fast contact force computation for nonpenetrating rigid bodies," *Proceedings of the 21st Annual Conference on Computer Graphics and Interactive Techniques, SIGGRAPH 1994*, pp. 23–34, 1994.
[14] M. Anitescu, F. A. Potra, and D. E. Stewart, "Time-stepping for three-dimensional rigid body dynamics," *Computer Methods in Applied Mechanics and Engineering*, vol. 177, pp. 183–197, Jul. 1999.
[15] E. Guendelman, R. Bridson, and R. Fedkiw, "Nonconvex rigid bodies with stacking," *ACM Trans. Graph.*, vol. 22, no. 3, pp. 871–878, 2003.
[16] D. M. Kaufman, S. Sueda, D. L. James, and D. K. Pai, "Staggered projections for frictional contact in multibody systems," *ACM Trans. Graph.*, vol. 27, no. 5, pp. 1–11, 2008.
[17] M. Müller, B. Heidelberger, M. Hennix, and J. Ratcliff, "Position based dynamics," *J. Vis. Comun. Image Represent.*, vol. 18, no. 2, pp. 109–118, 2007.
[18] M. Servin and C. Lacoursière, "Rigid body cable for virtual environments," *IEEE Transactions on Visualization*, vol. 14, no. 4, pp. 783–796, 2008.
[19] M. Servin and C. Lacoursière, "Massless cable for real-time simulation," *Computer Graphics Forum*, vol. 26, no. 2, pp. 172–184, 2007.
[20] I. García-Fernandez, M. Pla-Castells, and R. J. Martínez-Dura, "Elevation cable modeling for interactive simulation of cranes," in *2008 ACM SIGGRAPH / Eurographics Symposium on Computer Animation*, Jul. 2008, pp. 173–182.
[21] M. Servin, C. Lacoursière, and F. Nordfelth, "Adaptive resolution in physics based virtual environments," *SIGRAD 2008, Stockholm, Sweden*, 2008.
[22] C. Lacoursière, "Ghosts and machines: Regularized variational methods for interactive simulations of multibodies with dry frictional contacts," Ph.D. dissertation, Department of Computing Science, Umeå University, Sweden, SE-901 87, Umeå, Sweden, Jun. 2007.
[23] R. Cottle, J. Pang, and R. Stone, *The linear complementarity problem*. Academic Pr.: Academic Press, 1992.
[24] A. Fetter and J. D. Walecka, *Theoretical Mechanics of Particles and Continua*. McGraw-Hill, 1980, pp. 108–119.
[25] J. W. Demmel, S. C. Eisenstat, J. R. Gilbert, X. S. Li, and J. W. H. Liu, "A supernodal approach to sparse partial pivoting," *SIAM J. Matrix Analysis and Applications*, vol. 20, no. 3, pp. 720–755, 1999.
[26] AgX, "Agx multiphysics toolkit," http://www.algoryx.se/.

Kenneth Bodin Kenneth Bodin is a researcher at High Performance Computing Center North at Umeå University and CEO at Algoryx Simulations. He completed his MSc at the physics department of Umeå University in 1989 and his PhLic in Theoretical Physics from Chalmers University of Technology in 1992. His research interests include computational physics, high performance computing, computer visualization and condensed matter physics.

Claude Lacoursière Claude Lacoursière is a research assistant at the department of Computing Science at Umeå University. He completed his MSc at the physics department of McGill University in 1993 and his PhD at Umeå University in 2007. He has 10 years of experience from research and development of industrial multibody system simulation. His research interests include physics motivated numerical methods for real-time integration of mechanical systems, especially contacting multibodies subject to dry friction.

Fredrik Nordfelth Fredrik Nordfelth is R&D engineer at Algoryx Simulations. He received his MSc degree in Engineering Physics in 2008 from Umeå University. Besides algorithmic modeling of mechanical systems he has an interest in image analysis.

Martin Servin Martin Servin is senior lecturer at the department of Physics at Umeå University. He received his MSc and PhD degrees in theoretical physics from Umeå University in 1999 and 2003, respectively. His research interests include modeling and numerical simulation of complex mechanical systems with particular interest for real-time interactive 3D graphics and applications to robotics, vehicle simulation and industrial processes.